Scientia Iranica D (2020) 27(6), 3190–3203

Sharif University of Technology
**Scientia Iranica**
*Transactions D: Computer Science & Engineering and Electrical Engineering*
http://scientiairanica.sharif.edu

*Research Note*

# Design and analysis of solar photovoltaic-fed Z-source inverter-based dynamic voltage restorer

**M. Prasad[a,*], A.K. Akella[b], and A.Y. Abdelaziz[c]**

a. *Department of Electrical Engineering, NIT Jamshedpur, Jharkhand, India.*
b. *Faculty of Engineering, Department of Electrical & Electronics Engineering, NIT Jamshedpur, India.*
c. *Faculty of Engineering, Department of Electrical Power & Machines, Ain Shams University, Cairo, Egypt.*

Received 24 May 2018; received in revised form 17 January 2019; accepted 18 February 2019

**KEYWORDS**
Dynamic voltage restorer;
Perturb & observe;
Maximum power point tracking.

**Abstract.** Z-Source Inverter (ZSI) is a new topology of power converter, especially a DC-AC converter, at a very interesting power level. For instance, it only uses a single-stage power converter with a buck-boost characteristic. This work introduced a combination of a solar system and a ZSI based dynamic voltage restorer to reduce the voltage swell and harmonics under sudden addition of a balanced three-phase nonlinear load. This paper focused on Perturb and Observe (P&O) algorithm to automatically determine the operating voltage of PV systems that would produce maximum power output. The proposed ZSI based dynamic voltage restorer was designed and modeled by using MATLAB/SIMULINK. The outcomes were compared with those of conventional dynamic voltage restorers equipped with voltage and current source inverters.



## 1. Introduction

Presently, in addition to quality problems, electric power systems face voltage waveforms including swells and sags as major constraints [1,2]. The performance of power systems can be enhanced by incorporating some controllable custom power devices such as dynamic voltage restorers equipped with voltage source, current source, and Z-Source Inverters (ZSI) [3–5]. The disadvantages of conventional dynamic voltage restorer with voltage and current source inverters were enumerated in [6–8]. ZSI can be used to enhance the boost operation for the inverter AC output voltage and therefore, inverters can operate in the shoot-through mode [9]. Unlike conventional inverters such as voltage and current sources, the short-circuit mode is not destructive and has been truly used in the ZSI [5]. Solar energy is one of the most reliable sources of renewable energy power generation [10]. Energy from sunlight is converted through the power conversion process so that the generated power can be transferred to an existing electrical network. The circuit of conventional PV power converters requires two-stage converters: first, it steps up the solar voltage and then, changes direct current input back into alternator current before it can be fed into the existing electrical grid [11,12]. However, a ZSI uses a single-stage power converter with buck-boost characteristic [13]. Since ZSI is a new inverter type, it has received much academic spotlight. However, these techniques could not function well if the Perturb and Observe (P&O) algorithm has not been modified in advance to obtain greater voltage and current from the solar system and maintain the voltage at the DC-link of the inverter input [14–16]. This work introduces a combination of a solar system and

*. *Corresponding author. Tel.: +91-7993877167;*
*Fax: 916572382246*
*E-mail addresses: 2013pgphdee05@nitjsr.ac.in (M. Prasad); akakella@nitjsr.ac.in (A.K. Akella); almoatazabdelaziz@hotmail.com (A.Y. Abdelaziz)*

doi: 10.24200/sci.2019.51096.2000

a dynamic voltage restorer with ZSI for ameliorating distorted voltage and current waveforms in the process of switching a three-phase balanced nonlinear load. In this paper, the Maximum Power Point Tracking (MPPT) method such as P&O is applied to acquiring optimum power from the solar system. The proposed dynamic voltage restorer equipped with ZSI is validated in MATLAB/SIMULINK software and obtained outcomes are compared with the classical dynamic voltage restorer with voltage and current source inverters.

## 2. Dynamic voltage restorer with ZSI

Figure 1 shows the proposed Dynamic Voltage Restorer with a ZSI. The proposed system consists of a three-phase ZSI, interfacing inductance ($L_f$), a unit vector control technique, a DC source, and a solar photovoltaic system. A solar system is used to give DC supply to the DVR-based ZSI. The DVR with Z-source converts this DC supply to AC and ameliorates the voltage-related issues including voltage swells/sags in a distribution system under sudden switching of balanced three-phase nonlinear load.

## 3. Working principle of ZSI [6,8]

The working principle of ZSI can be explained in three different states such as active, zero, and shoot-through states, as highlighted in Figure 2(a)-(c). A detailed explanation of various working states of ZSI was given in [6–8]. The active state is additionally known as a non-shoot-through state, as given in Figure 2(c). In the shoot-through state, ZSI is working in one of the forty-one distinctive modes as shown in Figures 2(b) and 3 and Insulated-Gate Bipolar Transistor (IGBT) switches are short-circuited.

Let the impedance network elements have similar values ($L_1 = L_2 = L$ and $C_1 = C_1 = C$). Therefore, the Z-network inductor and capacitor voltage can be obtained using Eq. (1) [6,8]:

$$\left.\begin{aligned} v_{l1} &= v_{l2} = v_l \\ v_{c1} &= v_{c2} = v_c \end{aligned}\right\} \tag{1}$$

where $v_c$ is the capacitor voltage and $v_l$ is the inductor voltage of the ZSI. In the Shoot-Through (ST) state, $t_0$ is the time period and the relation between $v_c$ and $v_l$ is obtained through Eq. (2) [6,8]:

$$\left.\begin{aligned} v_l &= v_c \\ v_{dio} &= 2v_c \\ v_{in} &= 0 \ (ST \text{ state}) \end{aligned}\right\} \tag{2}$$

where $v_{in}$ and $v_{dio}$ are the dc-link input voltage of the inverter and diode voltage. In active and zero states, the relation between $v_c$ and $v_l$ is obtained using Eq. (3) and $t_1$ is the time interval:

$$\left.\begin{aligned} v_l &\neq v_c \\ v_{dio} &= v_{pv} = v_l + v_c \\ v_l &= v_{pv} - v_c = v_c - v_{in} \\ v_{in} &= v_c - v_l = 2v_c - v_{pv} \end{aligned}\right\} \tag{3}$$

where $v_{pv}$ is the output voltage of PV system. The

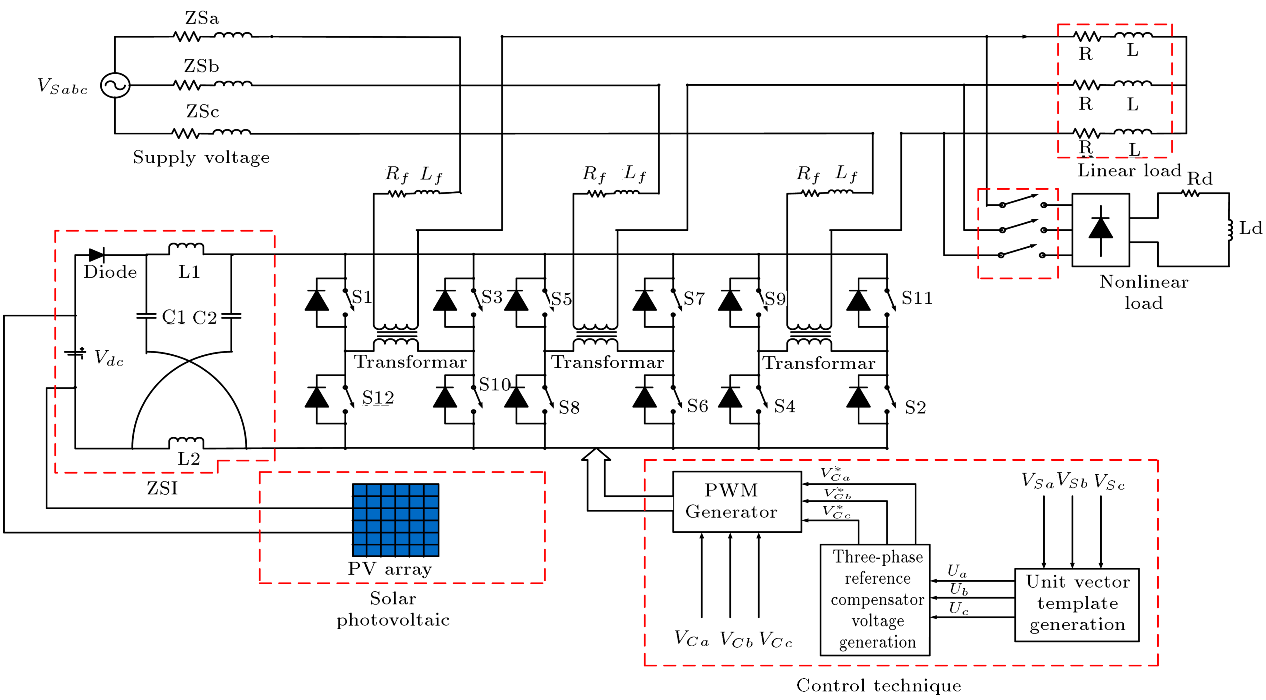


**Figure 1.** Combination of dynamic voltage restorers with Z-source inverters.

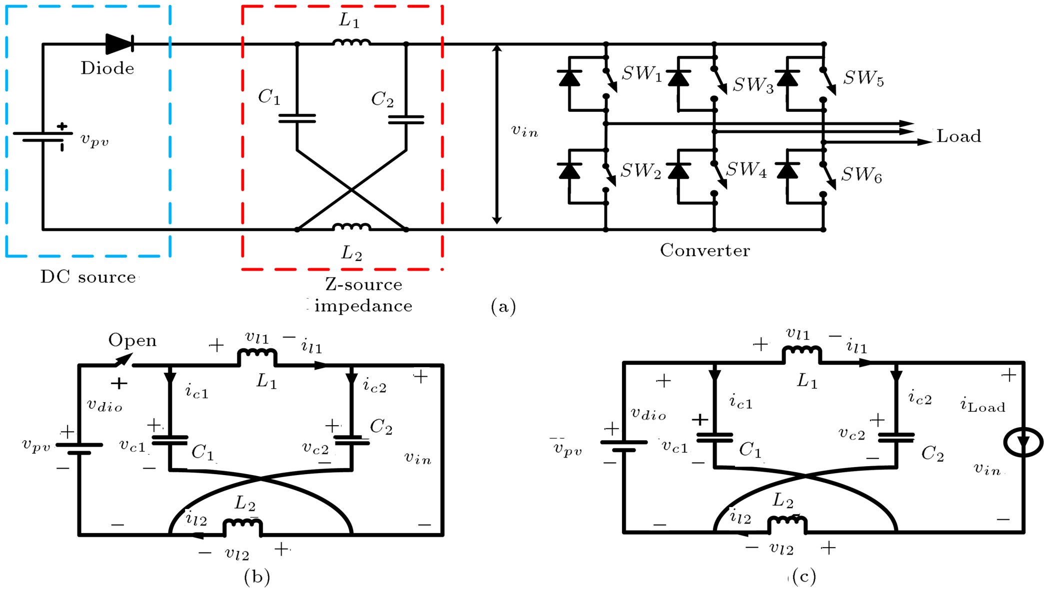


**Figure 2.** Z-Source Inverter (ZSI): (a) Configuration, (b) shoot-through state, and (c) active and zero states.

mean voltage of the Z-network inductor ($v_{l,\text{mean}}$) at time $t$ is expressed in Eq. (4) [6,8]:

$$v_{l,\text{mean}} = v_c * t_0 + (v_{pv} - v_c) * t_1 = 0,$$

$$v_c = v_{pv}\left(\frac{t_1}{t_1 - t_0}\right). \tag{4}$$

The mean input dc-link of the inverter is obtained through Eq. (5) ($v_{in}$):

$$v_{in} = t_0 * 0 + t_1\,(2v_c - v_{pv}) \quad \text{using Eq. (4)},$$

$$v_{in} = \left(\frac{t_1}{t_1 - t_0}\right) v_{pv} = v_c. \tag{5}$$

The input dc-link voltage of the inverter in active and zero states is expressed through Eq. (6):

$$\hat{v_{in}} = (v_c - v_l) = v_c - (v_{pv} - v_c)\,,$$

$$\hat{v_{in}} = (2v_c - v_{pv})\,. \tag{6}$$

By comparing Eqs. (4) and (6), Eq. (7) is obtained:

$$\hat{v_{in}} = \left(\frac{t}{t_1 - t_0}\right) v_{pv},$$

$$\hat{v_{in}} = bv_{pv}, \tag{7}$$

where '$b$' denotes the boost factor and is also obtained through Eq. (8):

$$b = \left(\frac{t}{t_1 - t_0}\right) = \frac{1}{1 - \left(\frac{2t_0}{t}\right)} \geq 1, \qquad t = t_0 + t_1. \tag{8}$$

The converter output voltage can be calculated using Eq. (9) [6,8]:

$$\hat{v_{ac}} = \frac{m\,\hat{v_{in}}}{2} = \left(\frac{mbv_{pv}}{2}\right), \tag{9}$$

where $m$ is the modulation index whose value should be less than or equal to one. The Z-network capacitor voltage can be obtained through Eqs. (10) and (11) [6,8]. From Eq. (4), we obtain the following:

$$v_c = \left(\frac{t_1}{t_1 - t_0}\right) v_{pv},$$

$$v_c = \left(\frac{t_1}{t}\right)\left(\frac{t}{t_1 - t_0}\right) v_{pv},$$

$$v_c = \left(\frac{1 - \left({}^{t_0}\!/_{t}\right)}{1 - \left({}^{2t_0}\!/_{t}\right)}\right) v_{pv}, \tag{10}$$

$$v_c = \frac{b+1}{2b} * b * v_{pv} = \left(\frac{b+1}{2}\right) v_{pv}. \tag{11}$$

## 4. Impedance source inverter design

### 4.1. Z-network inductor design

In active and zero modes, a mean current passing through the inductor is reduced, as expressed in Eq. (12) [6,8]:

$$i_{l,\text{mean}} = \left(\frac{p_{in}}{v_{pv}}\right). \tag{12}$$

For designing ZSI parameters such as inductor and capacitor, the 30% current ripples are taken.

The maximum current flowing through the inductor [6,8] is:

$$i_{l,\max} = i^{-}_{l,\text{mean}} + 30\% \text{ of } i^{-}_{l,\text{mean}}\,.$$

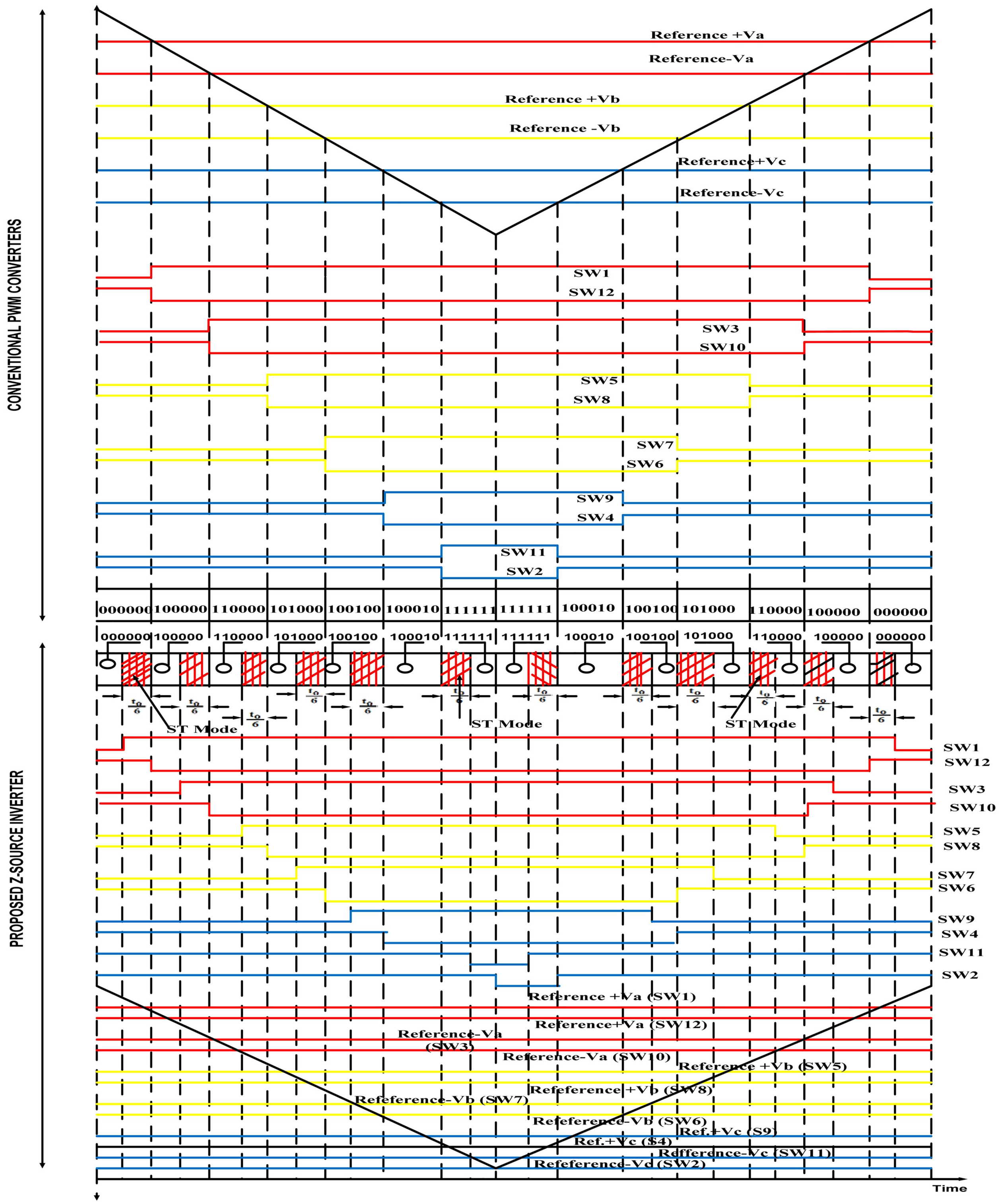

**Figure 3.** Modulation of the Z-Source Inverter (ZSI).

The minimum current flowing through the inductor [6,8] is given below:

$$i_{l,\min} = i^{-}_{l,\text{mean}} - 30\% \text{ of } i^{-}_{l,\text{mean}}.$$

In ST state, $v_l = v_c = v$, $v_l = v_c = v = \left(\frac{b+1}{2}\right) v_{pv}$, use the value of $v_c$ from Eq. (11).

The value of inductor is determined through Eq. (13):

$$L = \left(\frac{v * t_0}{\Delta i}\right), \tag{13}$$

where $\Delta i = (i_{l,\max} - i_{l,\min})$.

### *4.2. Z-source capacitor design*

The capacitor value is obtained through Eq. (14) [6,8]:

$$C = \left( \frac{\bar{i_{l,avg}} * t_0}{\Delta v_c} \right), \qquad \Delta v_c = v * 3\%. \tag{14}$$

In the ST state, the value of inductor and capacitor can be calculated by Eqs. (11) and (14) [6,8].

$$L = \left( \frac{v * t_0}{\Delta i} \right) = \left( \frac{167.75 * 9.83}{2.57} \right) = 0.6 \text{ mH},$$

$$C = \left( \frac{\bar{i_{l,\text{mean}}} * t_0}{\Delta v_c} \right) = \left( \frac{4.28 * 9.83}{844.20} \right) = 0.05\ \mu f.$$

### *4.3. Voltage gain*

The voltage gain can be expressed in Eq. (15) [8]:

$$G = m * b = (^{m}/\sqrt{3}m - 1),$$

$$G = \left[ ^{1}/_{2} * ^{D(1-D)}/_{2D - D(1-D) - 1} \right]. \tag{15}$$

### *4.4. Switching losses [8]*

The switching loss of each IGBT in active and ST states $P_{S-nst}$ and $P_{S-st}$ is calculated through Eqs. (16) and (17).

$$P_{S-nst} = {}^{1}/_{2\pi T_{SW}} \left( E_{SW-onn} + E_{SW-off} \right)$$
$$* \left( \int_0^{\pi} \text{Sin}x dx - \frac{1}{2} \int_{\frac{\pi}{6}-\phi}^{\frac{5\pi}{6}-\phi} |\text{Sin}x|\, dx \right), \tag{16}$$

$$P_{S-st} = {}^{1}/_{2T_{SW}} \left( E_{SW-ons} + E_{SW-offs} \right). \tag{17}$$

$E_{SW-on}$ and $E_{SW-off}$ are the switch-on and switch-off energy losses of the IGBT at peak current, respectively. $E_{SW-ons}$ and $E_{SW-offs}$ are the switch-on and switch-off energy losses corresponding to the mean turn on current of the shoot-through states, which is $\frac{2}{3}I_L$.

### *4.5. Voltage stress across the devices [8]*

According to Eq. (7), the voltage stress, $S_S$, can be expressed in Eq. (18):

$$S_S = v_{in} = bv_{pv}. \tag{18}$$

## 5. Modulation algorithm with timing diagram of the ZSI

Figure 3 outlines the structure of the eighty-three IGBT switching modes of the proposed ZSI including forty active modes, two zero modes, and forty-one ST modes. In active and zero modes, two IGBT switches with one, two, three, five, or six modes complement each other, similar to the commonly used traditional inverters and the proposed ZSI. However, forty-one ST modes with one (E1 to E6), two (E7 to E21), three (E22 to E31), four (E32 to E37), five (E38 to E40), or six legs (E41) are short circuited which are specific to ZSI. The switching states for the DVR with ZSI are shown in Table 1.

## 6. Unit Vector Template (UVT) control technique [17]

In UVT technique, first, three-phase supply voltages are measured and multiplied by $g = \frac{1}{V_{mag}}$, as shown in Figure 4, where $V_{mag}$ is the input voltage obtained through Eq. (19) [17].

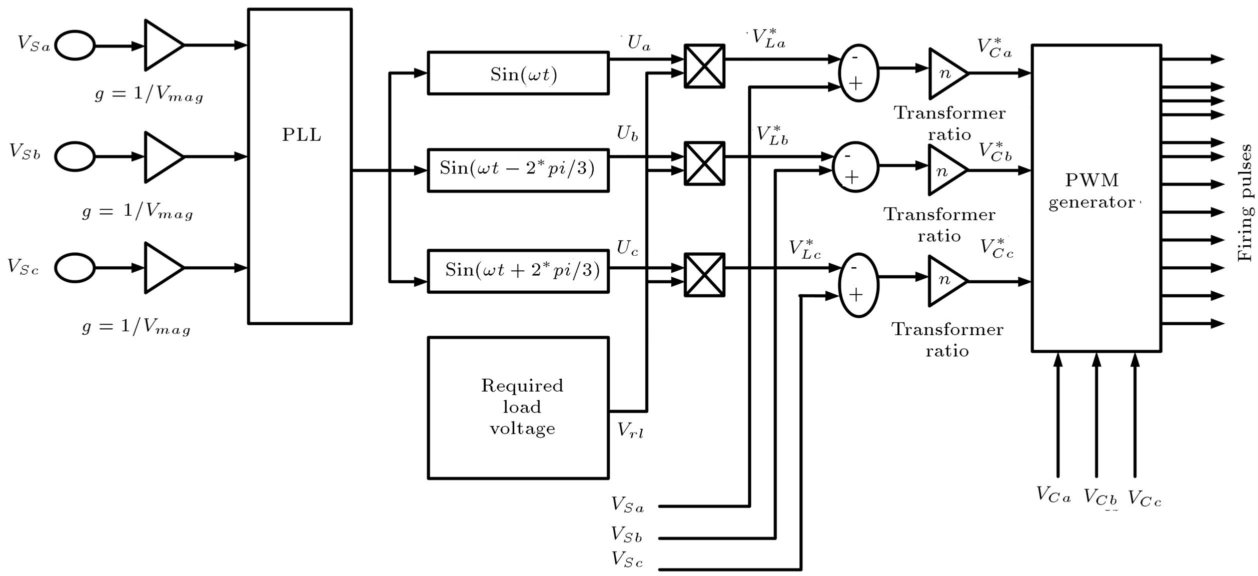


**Figure 4.** Schematic diagram of a control algorithm.

**Table 1.** Switching states of the proposed DVR with Z-Source Inverter (ZSI) (!SWY is the complement of SWY, where $Y = 1$, 3, 5, 7, 9, or 11).

| State {100000} (finite) | SW1 | SW12 | SW3 | SW10 | SW5 | SW8 | SW7 | SW6 | SW9 | SW4 | SW11 | SW2 |
|---|---|---|---|---|---|---|---|---|---|---|---|---|
| State {110000} (finite) | 1 | 0 | 0 | 1 | 0 | 1 | 0 | 1 | 0 | 1 | 0 | 1 |
| State {101000} (finite) | 1 | 0 | 1 | 0 | 0 | 1 | 0 | 1 | 0 | 1 | 0 | 1 |
| State {100100} (finite) | 1 | 0 | 0 | 1 | 1 | 0 | 0 | 1 | 0 | 1 | 0 | 1 |
| State {100010} (finite) | 1 | 0 | 0 | 1 | 0 | 1 | 0 | 1 | 1 | 0 | 0 | 1 |
| State {100001} (finite) | 1 | 0 | 0 | 1 | 0 | 1 | 0 | 1 | 0 | 1 | 1 | 0 |
| State {010000} finite | 0 | 1 | 1 | 0 | 0 | 1 | 0 | 1 | 0 | 1 | 0 | 1 |
| State {011000} finite | 0 | 1 | 1 | 0 | 1 | 0 | 0 | 1 | 0 | 1 | 0 | 1 |
| State {010100} finite | 0 | 1 | 1 | 0 | 0 | 1 | 1 | 0 | 0 | 1 | 0 | 1 |
| State {010010} finite | 0 | 1 | 1 | 0 | 0 | 1 | 0 | 1 | 1 | 0 | 0 | 1 |
| State {010001} finite | 0 | 1 | 1 | 0 | 0 | 1 | 0 | 1 | 0 | 1 | 1 | 0 |
| State {001000} finite | 0 | 1 | 0 | 1 | 1 | 0 | 0 | 1 | 0 | 1 | 0 | 1 |
| State {001100} finite | 0 | 1 | 0 | 1 | 1 | 0 | 1 | 0 | 0 | 1 | 0 | 1 |
| State {001010} finite | 0 | 1 | 0 | 1 | 1 | 0 | 0 | 1 | 1 | 0 | 0 | 1 |
| State {001001} finite | 0 | 1 | 0 | 1 | 1 | 0 | 0 | 1 | 0 | 1 | 1 | 0 |
| State {000100} finite | 0 | 1 | 0 | 1 | 0 | 1 | 1 | 0 | 0 | 1 | 0 | 1 |
| State {000110} finite | 0 | 1 | 0 | 1 | 0 | 1 | 1 | 0 | 1 | 0 | 0 | 1 |
| State {000101} finite | 0 | 1 | 0 | 1 | 0 | 1 | 1 | 0 | 0 | 1 | 1 | 0 |
| State {000010} finite | 0 | 1 | 0 | 1 | 0 | 1 | 0 | 1 | 1 | 0 | 0 | 1 |
| State {000011} finite | 0 | 1 | 0 | 1 | 0 | 1 | 0 | 1 | 1 | 0 | 1 | 0 |
| State {111000} finite | 1 | 0 | 1 | 0 | 1 | 0 | 0 | 1 | 0 | 1 | 0 | 1 |
| State {110100} finite | 1 | 0 | 1 | 0 | 0 | 1 | 1 | 0 | 0 | 1 | 0 | 1 |
| State {110010} finite | 1 | 0 | 1 | 0 | 0 | 1 | 0 | 1 | 1 | 0 | 0 | 1 |
| State {110001} finite | 1 | 0 | 1 | 0 | 0 | 1 | 0 | 1 | 0 | 1 | 1 | 0 |
| State {011100} finite | 0 | 1 | 1 | 0 | 1 | 0 | 1 | 0 | 0 | 1 | 0 | 1 |
| State {011010} finite | 0 | 1 | 1 | 0 | 1 | 0 | 0 | 1 | 1 | 0 | 0 | 1 |
| State {011001} finite | 0 | 1 | 1 | 0 | 1 | 0 | 0 | 1 | 0 | 1 | 1 | 0 |
| State {001110} finite | 0 | 1 | 0 | 1 | 1 | 0 | 1 | 0 | 1 | 0 | 0 | 1 |
| State {001101} finite | 0 | 1 | 0 | 1 | 1 | 0 | 1 | 0 | 0 | 1 | 1 | 0 |
| State {000111} finite | 0 | 1 | 0 | 1 | 0 | 1 | 1 | 0 | 1 | 0 | 1 | 0 |
| State {100011} finite | 1 | 0 | 0 | 1 | 0 | 1 | 0 | 1 | 1 | 0 | 1 | 0 |
| State {111100} finite | 1 | 0 | 1 | 0 | 1 | 0 | 1 | 0 | 0 | 1 | 0 | 1 |
| State {111010} finite | 1 | 0 | 1 | 0 | 1 | 0 | 0 | 1 | 1 | 0 | 0 | 1 |
| State {111001} finite | 1 | 0 | 1 | 0 | 1 | 0 | 0 | 1 | 0 | 1 | 1 | 0 |
| State {011110} finite | 0 | 1 | 1 | 0 | 1 | 0 | 1 | 0 | 1 | 0 | 0 | 1 |
| State {011101} finite | 0 | 1 | 1 | 0 | 1 | 0 | 1 | 1 | 0 | 1 | 1 | 0 |
| State {001111} finite | 0 | 1 | 0 | 1 | 1 | 0 | 1 | 0 | 1 | 0 | 1 | 0 |
| State {100111} finite | 1 | 0 | 0 | 1 | 0 | 1 | 1 | 0 | 1 | 0 | 1 | 0 |
| State {111110} finite | 1 | 0 | 1 | 0 | 1 | 0 | 1 | 0 | 1 | 0 | 0 | 1 |
| State {011111} finite | 0 | 1 | 1 | 0 | 1 | 0 | 1 | 0 | 1 | 0 | 1 | 0 |
| Null {000000} (0 V) | 0 | 1 | 0 | 1 | 0 | 1 | 0 | 1 | 0 | 1 | 0 | 1 |
| Nul l{111111} (0 V) | 1 | 0 | 1 | 0 | 1 | 0 | 1 | 0 | 1 | 0 | 1 | 0 |
| Shoot-through E1 (0V) | 1 | 1 | SW3 | !SW3 | SW5 | !SW5 | SW7 | !SW7 | SW9 | !SW9 | SW11 | !SW11 |
| Shoot-through E2 (0V) | SW1 | !SW1 | 1 | 1 | S5 | !S5 | S7 | !S7 | S9 | !S9 | S11 | !S11 |
| Shoot-through E3 (0V) | SW1 | !SW1 | SW3 | !SW3 | 1 | 1 | SW7 | !SW7 | SW9 | !SW9 | SW11 | !SW11 |
| Shoot-through E4 (0V) | SW1 | !SW1 | SW3 | !SW3 | SW5 | !SW5 | 1 | 1 | SW9 | !SW9 | SW11 | !SW11 |
| Shoot-through E5 (0V) | SW1 | !SW1 | SW3 | !SW3 | SW5 | !SW5 | SW7 | !SW7 | 1 | 1 | SW11 | !SW11 |
| Shoot-through E6 (0V) | SW1 | !SW1 | SW3 | !SW3 | SW5 | !SW5 | SW7 | !SW7 | SW9 | !SW9 | 1 | 1 |
| Shoot-through E7 (0V) | 1 | 1 | 1 | 1 | SW5 | !SW5 | SW7 | !SW7 | SW9 | !SW9 | SW11 | !SW11 |
| Shoot-through E8 (0V) | 1 | 1 | SW3 | !SW3 | 1 | 1 | SW7 | !SW7 | SW9 | !SW9 | SW11 | !SW11 |

**Table 1.** Switching states of the proposed DVR with Z-Source Inverter (ZSI) (!SWY is the complement of SWY, where $Y = 1$, 3, 5, 7, 9, or 11) (continued).

| | | | | | | | | | | | | |
|---|---|---|---|---|---|---|---|---|---|---|---|---|
| Shoot-through E9 (0V) | 1 | 1 | SW3 | !SW3 | SW5 | !SW5 | 1 | 1 | SW9 | !SW9 | SW11 | !SW11 |
| Shoot-through E10 (0V) | 1 | 1 | SW3 | !SW3 | SW5 | !SW5 | SW7 | !SW7 | 1 | 1 | SW11 | !SW11 |
| Shoot-through E11 (0V) | 1 | 1 | SW3 | !SW3 | SW5 | !SW5 | SW7 | !SW7 | SW9 | !SW9 | 1 | 1 |
| Shoot-through E12 (0V) | SW1 | !SW1 | 1 | 1 | 1 | 1 | S7 | !SW7 | SW9 | !SW9 | SW11 | !SW11 |
| Shoot-through E13 (0V) | SW1 | !SW1 | 1 | 1 | SW5 | !SW5 | 1 | 1 | SW9 | !SW9 | SW11 | !SW11 |
| Shoot-throughE14 (0V) | SW1 | !SW1 | 1 | 1 | SW5 | !SW5 | SW7 | !SW7 | 1 | 1 | SW11 | !SW11 |
| Shoot-through E15 (0V) | SW1 | !SW1 | 1 | 1 | SW5 | !SW5 | SW7 | !SW7 | SW9 | !SW9 | 1 | 1 |
| Shoot-through E16 (0V) | SW1 | !SW1 | SW3 | !S3 | 1 | 1 | 1 | 1 | SW9 | !SW9 | SW11 | !SW11 |
| Shoot-through E17 (0V) | SW1 | !SW1 | SW3 | !S3 | 1 | 1 | SW7 | !SW7 | 1 | 1 | SW11 | !SW11 |
| Shoot-through E18 (0V) | SW1 | !SW1 | SW3 | !S3 | 1 | 1 | SW7 | !SW7 | SW9 | !SW9 | 1 | 1 |
| Shoot-through E19 (0V) | SW1 | !SW1 | SW3 | !S3 | SW5 | !SW5 | 1 | 1 | 1 | 1 | SW11 | !SW11 |
| Shoot-through E20 (0V) | SW1 | !SW1 | SW3 | !S3 | SW5 | !SW5 | 1 | 1 | SW9 | !SW9 | 1 | 1 |
| Shoot-through E21 (0V) | SW1 | !SW1 | SW3 | !S3 | SW5 | !SW5 | SW7 | !SW7 | 1 | 1 | 1 | 1 |
| Shoot-through E22 (0V) | 1 | 1 | 1 | 1 | 1 | 1 | SW7 | !SW7 | SW9 | !SW9 | SW11 | !SW11 |
| Shoot-through E23 (0V) | 1 | 1 | 1 | 1 | SW5 | !SW5 | 1 | 1 | SW9 | !SW9 | SW11 | !SW11 |
| Shoot-through E24 (0V) | 1 | 1 | 1 | 1 | SW5 | !SW5 | SW7 | !SW7 | 1 | 1 | SW11 | !SW11 |
| Shoot-through E25 (0V) | 1 | 1 | 1 | 1 | SW5 | !SW5 | SW7 | !SW7 | SW9 | !SW9 | 1 | 1 |
| Shoot-through E26 (0V) | SW1 | !SW1 | 1 | 1 | 1 | 1 | 1 | 1 | SW9 | !SW9 | SW11 | !SW11 |
| Shoot-through E27 (0V) | SW1 | !SW1 | 1 | 1 | 1 | 1 | SW7 | !SW7 | 1 | 1 | SW11 | !SW11 |
| Shoot-through E28 (0V) | SW1 | !SW1 | 1 | 1 | 1 | 1 | SW7 | !SW7 | SW9 | !SW9 | 1 | 1 |
| Shoot-through E29 (0V) | SW1 | !SW1 | SW3 | !SW3 | 1 | 1 | 1 | 1 | 1 | 1 | SW11 | !SW11 |
| Shoot-through E30 (0V) | SW1 | !SW1 | SW3 | !SW3 | 1 | 1 | 1 | 1 | SW9 | !SW9 | 1 | 1 |
| Shoot-through E31 (0V) | SW1 | !SW1 | SW3 | !SW3 | SW5 | !SW5 | 1 | 1 | 1 | 1 | 1 | 1 |
| Shoot-through E32 (0V) | 1 | 1 | 1 | 1 | 1 | 1 | 1 | 1 | SW9 | !SW9 | SW11 | !SW11 |
| Shoot-through E33 (0V) | 1 | 1 | 1 | 1 | 1 | 1 | SW7 | !SW7 | 1 | 1 | SW11 | !SW11 |
| Shoot-through E34 (0V) | 1 | 1 | 1 | 1 | 1 | 1 | SW7 | !SW7 | SW9 | !SW9 | 1 | 1 |
| Shoot-through E35 (0V) | SW1 | !SW1 | 1 | 1 | 1 | 1 | 1 | 1 | 1 | 1 | SW11 | !SW11 |
| Shoot-through E36 (0V) | SW1 | !SW1 | 1 | 1 | 1 | 1 | 1 | 1 | SW9 | !SW9 | 1 | 1 |
| Shoot-through E37 (0V) | SW1 | !SW1 | SW3 | !SW3 | 1 | 1 | 1 | 1 | 1 | 1 | 1 | 1 |
| Shoot-through E38 (0V) | 1 | 1 | 1 | 1 | 1 | 1 | 1 | 1 | 1 | 1 | SW11 | !SW11 |
| Shoot-through E39 (0V) | 1 | 1 | 1 | 1 | 1 | 1 | 1 | 1 | SW9 | !SW9 | 1 | 1 |
| Shoot-through E40 (0V) | S1 | !SW1 | 1 | 1 | 1 | 1 | 1 | 1 | 1 | 1 | 1 | 1 |
| Shoot-through E41 (0V) | 1 | 1 | 1 | 1 | 1 | 1 | 1 | 1 | 1 | 1 | 1 | 1 |

$$V_{mag} = \sqrt{(2/3)\left(V_{Sa}^2 + V_{Sb}^2 + V_{Sc}^2\right)}. \tag{19}$$

The voltage signals are given as an input into a Phase-Locked Loop (PLL). After receiving input signals, the PLL used to create unit vectors $U_a, U_b$, and $U_c$ is calculated using Eq. (20) [17]:

$$\left.\begin{array}{l} U_a = \mathrm{Sin}\,(\theta) \\ U_b = \mathrm{Sin}\,(\theta - 120) \\ U_c = \mathrm{Sin}\,(\theta + 120) \end{array}\right\}, \tag{20}$$

$V_{La}^*, V_{Lb}^*$, and $V_{Lc}^*$ are obtained by Eq. (21) [17]:

$$\begin{bmatrix} V_{La}^* \\ V_{Lb}^* \\ V_{Lc}^* \end{bmatrix} = [V_{rl}] \begin{bmatrix} U_a \\ U_b \\ U_c \end{bmatrix}. \tag{21}$$

The three-phase supply voltages are compared with $V_{La}^*, V_{Lb}^*$, and $V_{Lc}^*$, and the reference compensator voltage ($V_{Cabc}^*$) is generated. The Pulse Width Modulation (PWM) generator produces switching pulses after comparing the reference compensator voltages and used compensator voltages.

## 7. Perturb and Observe (P&O) algorithm [18–20]

The P&O technique is commonly known for hunting down the MPPT because it is straightforward and requires only an estimation of the voltage ($v_{pv}$) and current ($i_{pv}$) of the PV system [21]. P&O works by perturbing (increasing or decreasing) the measured photovoltaic voltage ($v_{pv}$) and comparing the instantaneous powers before and after perturbation [18–21]. The P&O algorithm is given in Figure 5.

## 8. Results and discussion

The proposed dynamic voltage restorer-based ZSI system in Figure 1 is modulated using MATLAB/SIMULINK under sudden switching of a balanced three-phase nonlinear load. Figure 6(a)-(c) shows different characteristics of the solar cell under sun irradiations. As the irradiation increases, the open-circuit voltage and the short-circuit current increase, as shown in Figure 6(a) and (b). Consequently, the P&O algorithm is used to obtain the highest amount of power from solar cells, as highlighted in Figure 7. The simulation specifications are shown in Table 2.

### *8.1. Swell alleviation by dynamic voltage restorer with voltage source inverter*

A 31% three-phase balanced voltage swell occurs on the supply side because of sudden switching of nonlinear load, as shown in Figure 8(a) and (b). At $t = 0.05$ to 0.15, a voltage source inverter-based DVR is connected to a distribution system and a compensated voltage is injected to compensate the three-phase balanced voltage swell, as shown in Figure 8(c). Figure 8(d) highlights the sinusoidal load voltage after minimizing the voltage swell effect. Figure 8(e) outlines the nature of the capacitor voltage of the dynamic voltage restorer equipped with source inverter.

### *8.2. Swell alleviation by dynamic voltage restorer with current source inverter*

Figure 9(a) and (b) show the voltage swell with a magnitude of 31% under sudden switching of three-phase balanced nonlinear load. It begins at $t = 0.05$ s and terminates at $t = 0.15$ s. Figure 9(c) depicts the ability of dynamic voltage restorer with a current source inverter to ameliorate the three-phase balanced

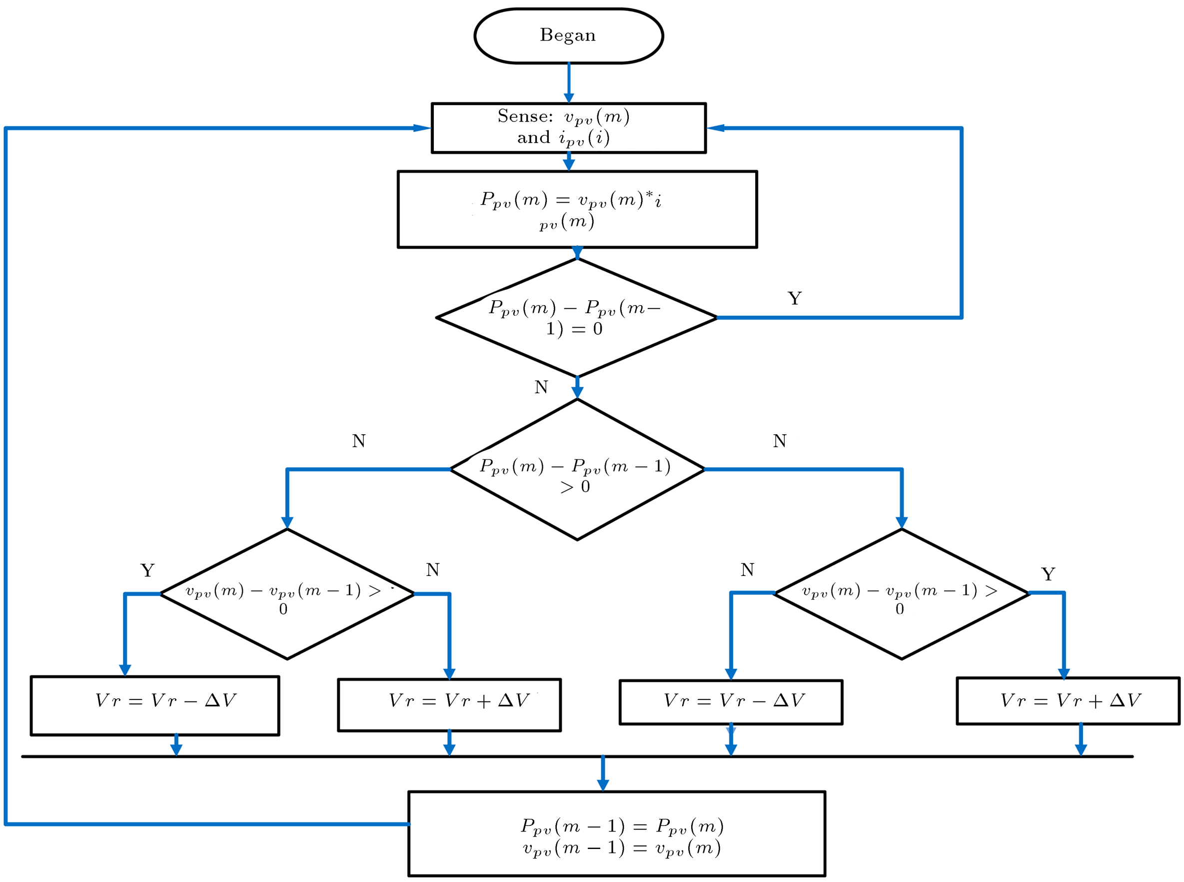


**Figure 5.** Perturb and observe algorithm.

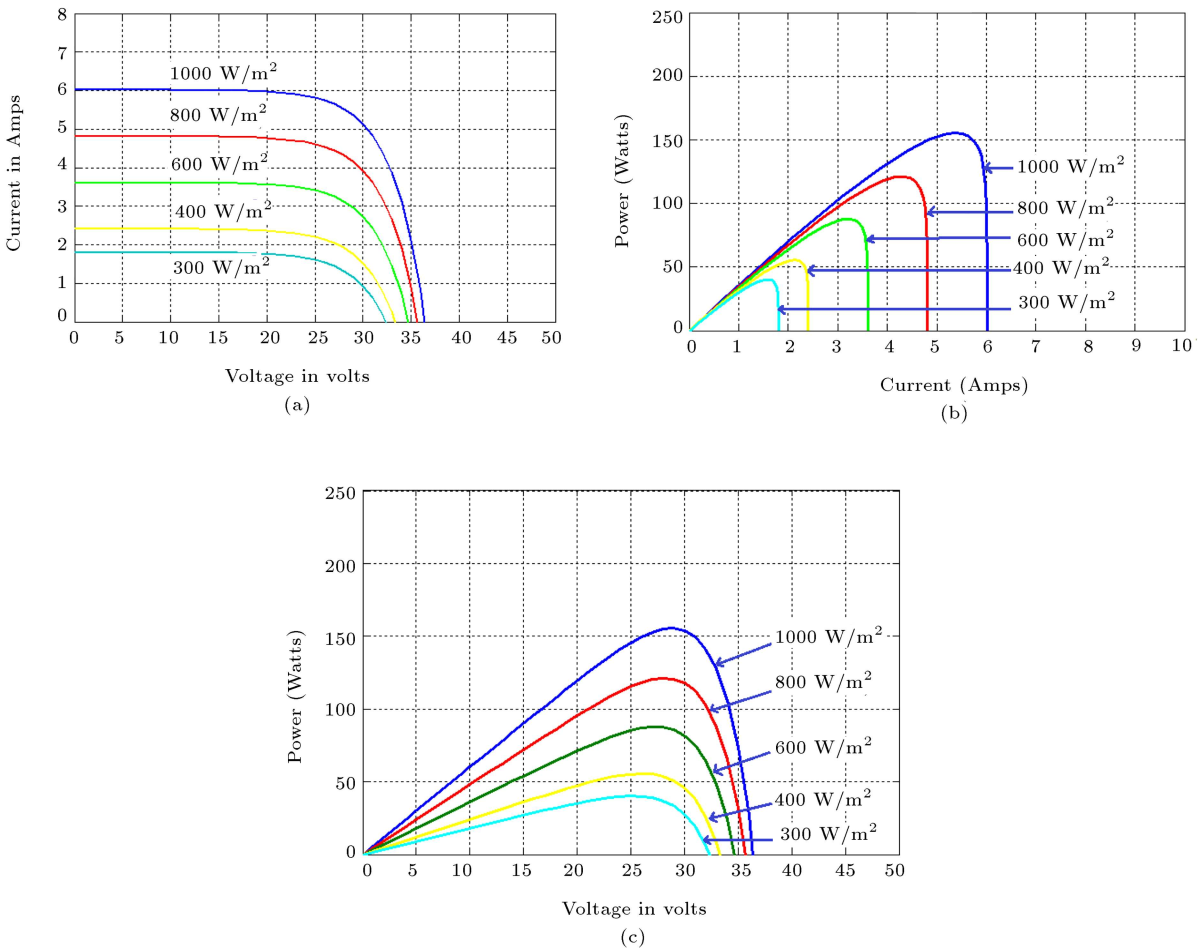


**Figure 6.** Characteristics of solar photovoltaic under different values of irradiation: (a) V-I characteristics, (b) P-I characteristics, and (c) P-V characteristics.

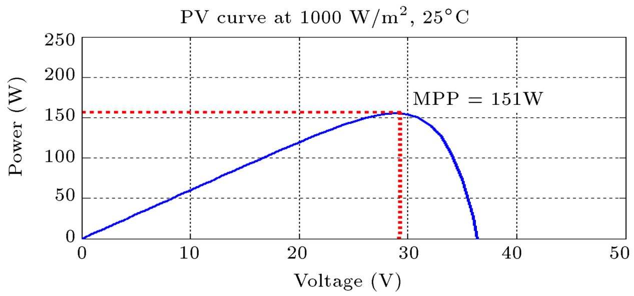


**Figure 7.** Perturb & Observe (P&O) algorithm.

voltage swell by injecting the compensated voltage. Figure 9(d) highlights the sinusoidal load voltage after minimizing the voltage swell effect. Figure 9(e) shows the behavior of inductor current of the dynamic voltage restorer with a current source inverter under voltage swell.

### 8.3. *Swell alleviation by dynamic voltage restorer with a ZSI*

Figure 10(a) and (b) show the voltage swell with a magnitude of 31% under sudden switching of three-phase balanced nonlinear load in a distribution network. It begins at $t = 50$ milliseconds and terminates at $t = 150$ milliseconds. Figure 10(c) depicts the ability of the dynamic voltage restorer with a ZSI to alleviate voltage swell by injecting the compensated voltage. Figure 10(d) highlights the sinusoidal load voltage after minimizing the voltage swell effect. Figure 10(e)–(f) outlines the nature of capacitor voltage and inductor current of the proposed dynamic voltage restorer based on ZSI.

## 9. Comparison of dynamic voltage restorers with voltage, current, and ZSI

Figure 11 outlines the comparison in compensated voltages of conventional dynamic voltage restorers with voltage, current, and proposed ZSI. Regardless of what inverters have been used, voltage swell with a magnitude of 31% (98 V) at $t = 0.5$ s for a duration of 0.35 s is observed. Therefore, the dynamic voltage restorers with inverters are associated with the system and they generate voltages of 132 V, 66.65 V, and 95

**Table 2.** DVR with Z-Source Inverter (ZSI) Specifications.

| **Parameters** | **Values** |
|---|---|
| Supply voltage (Vs) | 380 V |
| Frequency (f) | 50 Hz |
| Supply resistance (Rs) | 0.05 Ω |
| Supply inductance (Ls) | 3.5 $\mu$H |
| Linear load | Active power ($P$)= 5 kW<br>Inductive reactive power ($QL$) = 10 kVAR |
| Nonlinear load | Diode rectifier, $Rd = 10\ \Omega$, $Ld = 3\ \mu$H |
| Injection transformer | 240/120 V |
| DC-bus voltage (Vdc) | 150 V |
| Solar module | $V_{OC} = 36.1$ V<br>$I_{SC} = 6$ A<br>Number of solar cells ($C$) = 36<br>$P_{\max} = 151$ W<br>$V_{MPP} = 29.6$ V<br>$I_{MPP} = 5.1$ A<br>Diode identity factor ($n$) = 1<br>$R_s = 0.18\ \Omega$<br>$R_p = 360.002\ \Omega$<br>$L_I = L_2 = L = 0.6$ mH<br>$C_1 = C_2 = C = 0.05\ \mu$F<br>$m = 0.5$ |
| Z-source inverter | $t_0 = 9.83\ \mu$s<br>$I_{l,\text{avg}} = 4.28$ A<br>$I_{l,\max} = 5.56$ A<br>$i_{l,\min} = 2.99$ A<br>$\Delta i = 2.57$ A |

**Table 3.** Comparison of supply current THDi values.

| **Before compensation** | **DVR with VSI** | | **DVR with CSI** | | **Proposed DVR with ZSI** | |
|---|---|---|---|---|---|---|
| | **DVR with VSI (%)** | **Enhancement in THD$_i$ (%)** | **DVR with CSI (%)** | **Enhancement in THD$_i$ (%)** | **Proposed DVR with ZSI (%)** | **Enhancement in THD$_i$ (%)** |
| 7.97 | 0.65 | 91.8 | 0.75 | 90.58 | 0.5 | 93.72 |

V, respectively. The proposed dynamic voltage restorer with ZSI is characterized by better implementation than those with voltage and current source inverters, as highlighted in Figure 11.

Tables 3 and 4 show the capability of voltage, current, and proposed dynamic voltage restorers with ZSIs to eliminate current and voltage harmonics.

Total Harmonic Distortion (THD) of supply current without dynamic voltage restorers with voltage, current, and ZSIs connected to the system is measured as 7.97%; however, when they are connected to the system, the THDi values will be 0.65%, 0.75%, and 0.6%, as shown in Table 3. Therefore, a 93.72% decrease in THDi has been accomplished by the proposed dynamic voltage restorer with ZSI, compared with 91.8% and 90.58% decreases in THDi of voltage and current source inverters.

In Table 4, load voltage THDv is 18.62% when the

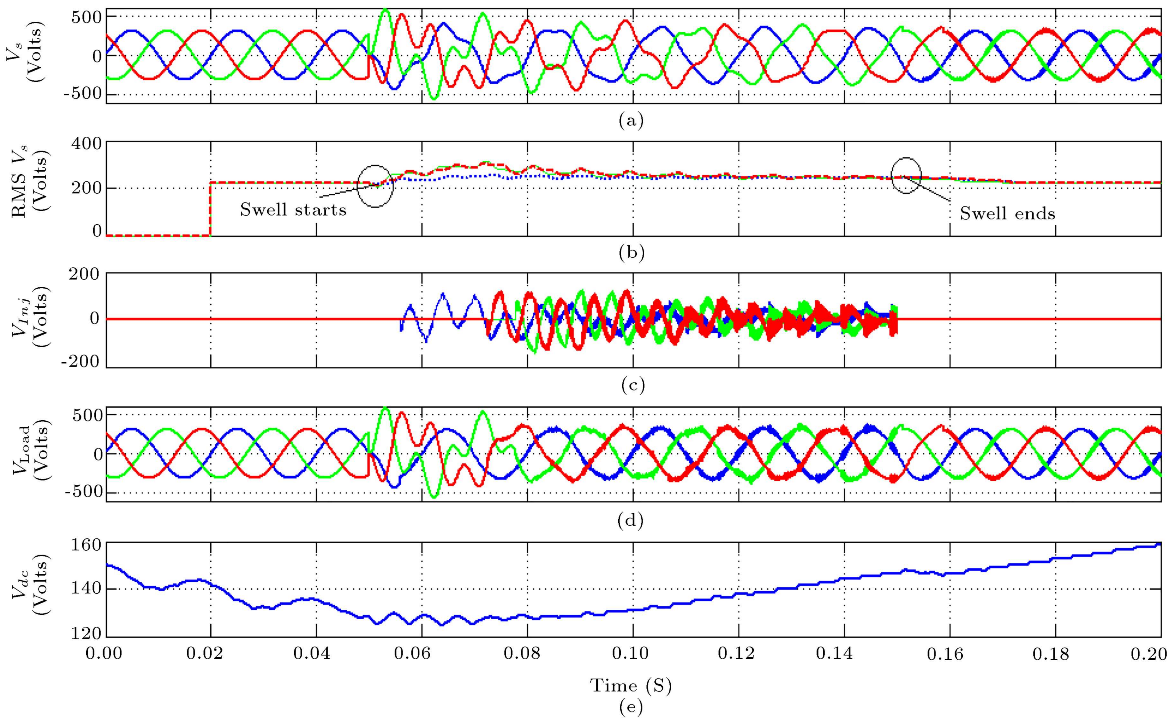


**Figure 8.** PV-VSI-DVR at 31% swell: (a) $V_S$, (b) RMS $V_S$, (c) $V_{\text{Inj}}$, (d) $V_{\text{Load}}$, and (e) $V_{dc}$.

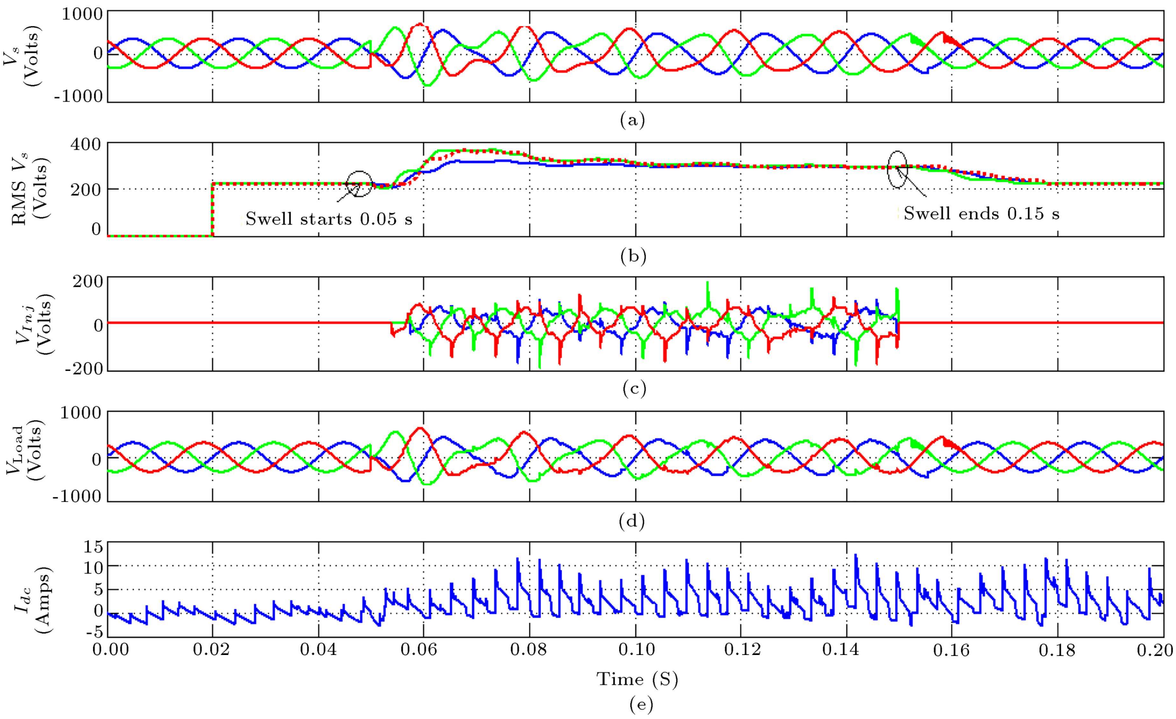


**Figure 9.** PV-CSI-DVR at 31% swell: (a) $V_S$, (b) $V_S$, (c) $V_{\text{Inj}}$, (d) $V_{\text{Load}}$, and (e) $I_{dc}$.

dynamic voltage restorers with voltage, current, and proposed ZSIs are not connected to the system. In contrast, when they are connected, the THDv values will be 3.5%, 2.48%, and 1.8%, as shown in Table 4. Therefore, a 90.33% decrease in THDi has been accomplished by the proposed dynamic voltage restorer with ZSI, compared with 81.2% and 86.68% decreases in THDv of voltage and current source inverters.

## 10. Conclusion

This work introduced a combination of a solar system

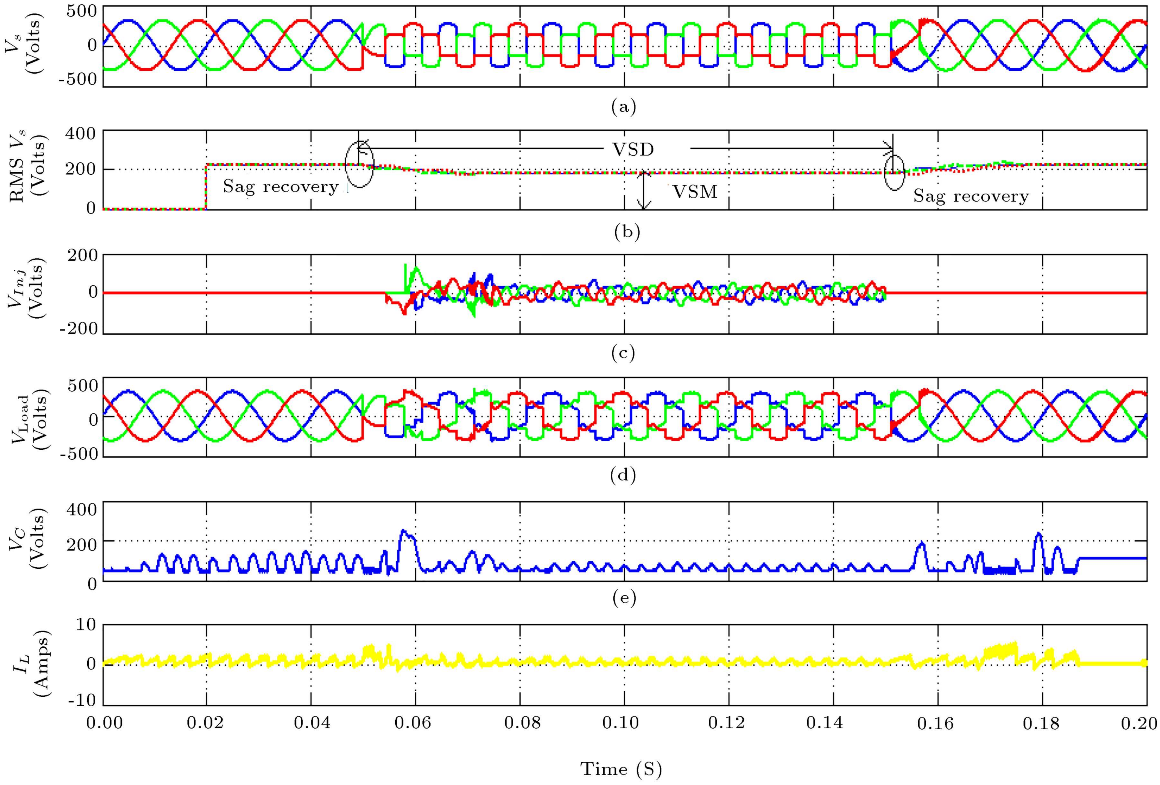


**Figure 10.** Proposed PV-ZSI-DVR at 31% swell: (a) $V_S$, (b) RMS $V_S$, (c) $V_{\text{Inj}}$, (d) $V_{\text{Load}}$, (e) $V_{dc}$, and (f) $I_{dc}$.

**Table 4.** Comparison of load voltage THDv values.

| Before compensation | DVR with VSI | | DVR with CSI | | Proposed DVR with ZSI | |
|---|---|---|---|---|---|---|
| | DVR with VSI (%) | Enhancement in THD$_v$ (%) | DVR with CSI (%) | Enhancement in THD$_v$ (%) | Proposed DVR with ZSI (%) | Enhancement in THD$_v$ (%) |
| 18.62 | 3.5 | 81.2 | 2.48 | 86.68 | 1.8 | 90.33 |

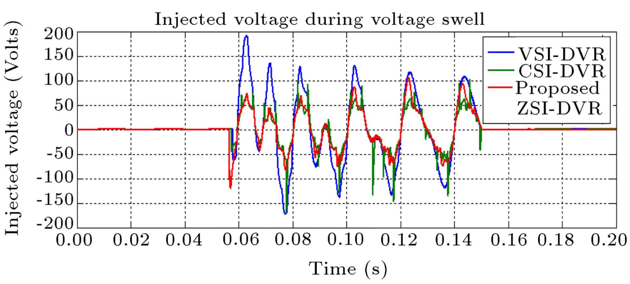


**Figure 11.** Compensated voltages.

and a dynamic voltage restorer with Z-source inverter for ameliorating voltage swell and harmonics under sudden addition of balanced three-phase nonlinear load. Results showed that in the swell condition, the proposed restorer could reduce possible voltage variations by injecting an exact magnitude of compensated voltage as compared to the conventional dynamic voltage restorers with voltage and current source inverters. Furthermore, results demonstrated the ability of the proposed restorer to eliminate current and voltage harmonics in the process of switching three-phase balanced nonlinear load, compared to the conventional dynamic voltage restorers with voltage and current source inverters. This study focused on Perturb and Observe (P&O) algorithm to automatically find the operating voltage of PV systems producing maximum power output.

## References

1. Santis, M.De., Noce, C., Varilone, P., et al. "Analysis of the origin of measured voltage sags in interconnected networks", *International Journal of Electric Power Systems Research*, **154**, pp. 391–400 (2018).

2. Nagata, E.A., Ferreira, D.D., Duque, C.A., et al.

"Voltage sag and swell detection and segmentation based on independent component analysis", *International Journal of Electric Power Systems Research*, **155**, pp. 274–280 (2018).

3. Wang, Y., Luo, H., and Xiao, X.Y. "Voltage sag frequency kernel density estimation method considering protection characteristics and fault distribution", *International Journal of Electric Power Systems Research*, **170**, pp. 128–137 (2019).
4. Nittala, R., Parimi, A.M., and Rao, K.U. "Comparing the performance of IDVR for mitigating voltage sag and harmonics with VSI and CSI as its building blocks", *IEEE International Conference on Signal Processing, Informatics, Communication and Energy Systems (SPICES)*, Kozhikode, pp. 1–5 (2015).
5. Balamurugan, M., Sivakumaran, T.S., and Devi, M.A. "Voltage sag/swell compensation using Z-source inverter DVR based on FUZZY controller", *IEEE International Conference on Emerging Trends in Computing, Communication and Nanotechnology (ICECCN)*, pp. 648–653 (2013).
6. Hanif, M., Basu, M., and Gaughan, K. "Understanding the operation of a Z-source inverter for photovoltaic application with a design example", *IET Power Electron*, **4**, pp. 278–287 (2011).
7. Zope, P.H. and Somkuwar, A. "Design and simualtion of single-phase Z-source inverter for utility interface", *International journal of Electrical Engineering and Technology*, **1**, pp. 127–143 (2012).
8. Pilehvar, M.S., Mardaneh, M., and Rajaei, A. "An analysis on the main formulas of Z-source inverter", *Scientia Iranica, Transactions D: Computer Science & Engineering and Electrical Engineering*, **22**(3), pp. 1077–1084 (2015).
9. Kannan, S.A., Rakesh, R., Amal, M.R., et al. "Performance analysis of PV single phase Z-source inverter", *International Journal of Innovative Research in Electrical, Electronics, Instrumentation and Control Engineering*, **2**, pp. 1069–1075 (2014).
10. Ali, U.S. "Impedance source converter for photovoltaic stand-alone system with vanadium redox flow battery storage", *Materials Today Proceedings*, **5**, pp. 241–247 (2018).
11. Umarani, D. and Seyezhai, R. "Modeling and control of quasi Z-source cascaded H-bridge multilevel inverter for grid connected photovoltaic systems", *Energy Procedia*, **90**, pp. 250–259 (2016).
12. Farhat, M., Barambones, O., and Sbita, L. "Efficiency optimization of a DSP-based standalone PV system using a stable single input fuzzy logic controller", *Renewable and Sustainable Energy Reviews*, **49**, pp. 907–920 (2015).
13. Carrasco, M. and Mancilla-David, F. "Maximum power point tracking algorithms for single-stage photovoltaic power plants under time-varying reactive power injection", *Solar Energy*, **132**, pp. 321–331 (2016).
14. Kandemir, E., Cetin, N.S., and Borekci, S. "A comprehensive overview of maximum power extraction methods for PV systems", *Renewable and Sustainable Energy Reviews*, **78**, pp. 93–112 (2017).
15. Gheibi, A., Mohammadi, S.M.A., and Farsangi, M.M. "A proposed maximum power point tracking by using adaptive fuzzy logic controller for photovoltaic systems", *Scientia Iranica, Transactions D: Computer Science & Engineering and Electrical Engineering*, **23**, pp. 1272–1281 (2016).
16. Kermadi, M. and Berkouk, E.M. "Artificial intelligence-based maximum power point tracking controllers for photovoltaic systems: comparative study", *Renewable and Sustainable Energy Reviews*, **69**, pp. 369–386 (2017).
17. Bouzelata, Y., Kurt, E., Chenni, R., et al. "Design and simulation of a unified power quality conditioner fed by solar energy", *International Journal of Hydrogen Energy*, **40**, pp. 15267–15277 (2015).
18. Ahmed, J. and Salam, Z. "A modified P&O maximum power point tracking method with reduced steady state oscillation and improved tracking efficiency", *IEEE Transaction on Sustainable Energy*, **7**, pp. 1506–1515 (2016).
19. Alik, R. and Jusoh, A. "An enhanced P&O checking algorithm MPPT for high tracking efficiency of partially shaded PV module", *Solar Energy*, **163**, pp. 570–580 (2018).
20. Ahmed, J. and Salam, Z. "An improved perturb and observe (P&O) maximum power point tracking (MPPT) algorithm for higher efficiency", *Applied Energy*, **150**, pp. 97–108 (2015).
21. Islam, F.R., Prakash, K., Mamun, K.A., et al. "Design of an optimum MPPT Controller for solar energy system", *Indonesian Journal of Electrical Engineering and Computer Science*, **2**, pp. 545–553 (2016).

## Biographies

**Miska Prasad** was born in India and received BE in Electrical & Electronics Engineering from GITAM University, Andhra Pradesh, India, and MTech in Power Systems from NIT Jamshedpur, Jharkhand, India in 2010 and 2013, respectively. Currently, he is pursuing PhD degree at Electrical Engineering Department, NIT Jamshedpur, India. His main research interests are power quality, custom power devices, and power electronics.

**Ashok Kumar Akella** was born in India, received the BSc (Engineering) and MTech (Control System) degrees from MIT Muzaffarpur, India in 1987 and 1992, respectively, completed his PhD (Renewable Energy System) from IIT Roorkee, India in 2006. He is a life member of ISTE. Since 1996, he has been serving as a faculty member at the Department of Electrical Engineering, NIT Jamshedpur, Jharkhand, India. His main research interests are control system, renewable energy system, and power quality.

**Almoataz Y. Abdelaziz** received the BSc and MSc degrees in Electrical Engineering from Ain Shams University, Cairo, Egypt in 1985 and 1990, respectively and PhD degree in Electrical Engineering according to the channel system between Ain Shams University, Egypt, and Brunel University, U.K., in 1996. He is currently a Professor of Electrical Power Engineering at Ain Shams University. Dr. Abdelaziz is the Chair of IEEE Education Society chapter in Egypt, a senior editor of Ain Shams Engineering Journal, an editor of Electric Power Components & Systems Journal, a member of editorial board, and a reviewer of technical papers in several international journals and conferences. He is a senior member in IEEE, a member in IET, and a part of Egyptian Sub-Committees of IEC and CIGRE. He has been awarded many prizes for distinct research and for international publishing from Ain Shams University, Egypt. He has authored or coauthored more than 300 refereed journal and conference papers in his research areas, which include the applications of artificial intelligence as well as evolutionary and heuristic optimization techniques to power system operation, planning, and control.